ASME 2009 International Design Engineering Technical Conferences (IDETC) & Computers and Information in Engineering Conference (CIE)
August 30 - September 2, 2009, San Diego, CA, USA

INDUCTION MOTOR MULTI-FAULT ANALYSIS BASED ON INTRINSIC MODE FUNCTIONS IN HILBERT-HUANG TRANSFORM

Xin Xue
Department of Mechanical Engineering
Email: xxue@engr.ucr.edu

V. Sundararajan
Department of Mechanical Engineering
Email: vsundar@engr.ucr.edu
Phone: 951-827-2446

Integrated Design and Manufacturing Laboratory
University of California, Riverside, Riverside, CA 92521, U.S.A

ABSTRACT

This paper reports experimental studies to detect two faults in a 3-phase 1.5hp induction motor using intrinsic mode functions from Hilbert-Huang transform. The faults studied are the eccentricity of the air-gap between the rotor and stator and damage to the outer race of bearings. The experiments are conducted under four conditions: the normal no-fault condition, two single fault conditions and the multiple faults condition. Two microphones, one vibration sensor and one current sensor are used to collect sound, vibration and current data respectively. The data is analyzed using the Hilbert-Huang transform and Fast Fourier Transform. Features are extracted from the spectrum of intrinsic mode functions and the average value of their envelope. Three simple classifiers are used to classify these four experimental conditions. The results demonstrate that the multiple sensors do improve the classification rate and that the Intrinsic Mode Functions obtained by the Hilbert-Huang transform are more effective than FFT in classifying multiple faults.

1. INTRODUCTION

The detection of incipient faults in induction motors has been the subject of research in modeling, fault simulation and feature extraction. Cameron et al [1] derived the frequency, principal slot harmonic, in current and vibration that result from eccentricity of the air-gap between the stator and rotor. Dorrell et al [2] observed that low frequency components near the fundamental of the current signal can be used to detect both static and dynamic eccentricity. The characteristic defect frequencies of rolling bearing can show in the vibration spectrum [3, 4], and in the current spectrum[5].

The technique most frequently used to detect frequencies is the Fast Fourier Transform (FFT). However, this method has a number of deficiencies when directly used over a faulty motor's vibration signature [6]. FFT alone is not capable of analyzing the frequency content of a defective bearing signal because such a signal is amplitude-modulated and non-stationary in nature. Wavelet transform is one of the most suitable time-frequency approaches. The problem is the fixed scale frequency resolution and its large computational time [7]. It depends on a single fixed type of mother wavelet chosen arbitrarily. Hilbert-Huang transform (HHT) provides multi-resolution in various frequency scales and takes the signal's frequency content and their variation into consideration [6, 8]. The implementation of HHT for bearing fault diagnosis has been reported by Hui and Haiqi [9] and Rai and Mohanty [7]. Hui analyzed the envelope of vibration signal and using marginal spectrum of IMFs to detect the fault defect frequencies. Rai compared the original vibration spectrum of vibration signal and the FFT of the decomposed signals for an outer race fault bearing and an inner race fault bearing. Their results demonstrate that the HHT is a promising method for bearing fault diagnosis.

This paper studies the vibration, current and sound signature of an induction motor under 4 conditions – a normal no-fault control condition, one bearing fault condition, one air-gap eccentricity condition and a multi-fault condition. Section 2 and 3 describes the definition of intrinsic mode functions and the process to extract the intrinsic mode functions. Section 4 describes the methodology and Section 5 discusses the results.

2. INTRINSIC MODE FUNCTIONS

2.1 Definition of Intrinsic mode functions (IMFs)

Huang et al [10, 11] have defined Intrinsic Mode Functions (IMFs) as a class of functions that satisfy two conditions:

(1) In the whole data set, the number of extrema and the number of zero-crossings must be either equal or differ at most by one. (In other words, every adjacent local maxima and minima of the wave must across the zero line.)
(2) At any point, the mean value of the envelope defined by the local maxima and the envelope defined by the local minima is zero. (In other words, the upper envelope and the lower envelope estimated from the local maxima and local minima are approximately symmetric with regard to the zero line.)

The next section explains the process to obtain IMFs called empirical mode decomposition.

2.2 Empirical mode decomposition

To extract IMFs from the signal $x(t)$, a sifting process comprises the following steps:
1) Find the positions and amplitudes of local maxima, and local minima of $x(t)$. Then create an upper envelope by cubic spline interpolation of the local maxima, and a lower envelope by cubic spline interpolation of the local minima. Calculate the mean $m_1(t)$ of the upper and lower envelopes. Subtracting the envelope mean signal from the original input signal, we have

$$h_1(t) = x(t) - m_1(t) \tag{1}$$

Check whether $h_1(t)$ meets the requirements to be an IMF. If not, treat $h_1(t)$ as new data and repeat the previous process. Then set

$$h_{11}(t) = h_1(t) - m_{11}(t) \tag{2}$$

Repeat this sifting procedure k times until $h_{1k}(t)$ is an IMF; this is designated as the first IMF.

$$c_1(t) = h_{1k}(t) \tag{3}$$

2) Subtract $c_1(t)$ from the input signal and define the remainder, $r_1(t)$, as the first residue. Since the residue, $r_1(t)$, still contains information related to longer period components, it is taken as a new data stream. Repeat the above-described sifting process to find more IMFs until the stopping criteria are met. The sifting process is stopped when either of criteria are met: 1) the component $c_n(t)$, or the residue $r_n(t)$, becomes so small in magnitude as to be considered inconsequential, or 2) the residue, $r_n(t)$, becomes a monotonic function from which an IMF cannot be extracted. Finally, the signal can be represented as the sum of IMFs and a residue.

$$x(t) = \sum_{j=1}^{n} c_j(t) + r_n(t) \tag{4}$$

2.3 Envelope of IMFs and instantaneous frequency

Apply the Hilbert transform to all the IMFs, $c_j(t)$, we have

$$H[c_j(t)] = \frac{1}{\pi}\int_{-\infty}^{+\infty} \frac{c_j(t)}{t-\tau} d\tau \tag{5}$$

After the Hilbert transform, a complex signal is formed as

$$z_j(t) = c_j(t) + i\, H[c_j(t)]$$

Expressing $z_j(t)$ in complex exponential form

$$z_j(t) = a_j(t) e^{i\theta_j(t)} \tag{6}$$

where the amplitude, the envelope,

$$a_j(t) = \sqrt{c_j(t)^2 + H[c_j(t)]^2} \tag{7}$$

and the phase angle

$$\theta_j(t) = \arctan\left(\frac{H[c_j(t)]}{c_j(t)}\right) \tag{8}$$

Then the instantaneous frequency is

$$\omega_j(t) = \frac{d\theta_j(t)}{dt} \tag{9}$$

Thus the original signal can be expressed as

$$x(t) = \sum_{j=1}^{n} a_j(t) e^{i\int \omega_j(t) dt}$$

where the residue has been left out, and the expression represents a generalized Fourier expansion.

3. FEATURES EXTRACTED FROM IMFS

Ideally, even with multi-faults present in the system, the single fault characteristic frequencies will be present. By inspecting the FFT of each IMF, those fault characteristic frequencies can be found in the IMFs and the magnitude can be used as features.

For a rolling element bearing, the outer race fault characteristic frequency is [12]:

$$f_o = \frac{n}{2}\left(1 - \frac{d}{D}\cos\,\beta\right) f_r \tag{10}$$

where n is the number of balls, d is the ball diameter, D is the pitch diameter, β is the contact angle, and f_r is the rotation speed of the rotor. If a current sensor is used on the supply line or an audio sensor is used to collect the sound signals from the motor, the corresponding current and sound spectra show the fault characteristic frequency [5, 12]

$$f = f_1 \pm f_o$$

where f_1 is the power supply frequency.

For air gap eccentricity fault, the principal slot harmonic (PSH) frequency is calculated by [1, 12]

$$f = \left(\frac{1-s}{p}(kR \pm n_d) \pm v\right) f_1$$

where s is the slip of the rotor, p is number of pole pairs, R is number of rotor bars, $n_d = 0$ in case of static eccentricity, and n_d =1,2,3… in case of dynamic eccentricity, k is an integer, v =1,3,5,… Low frequency components near the fundamental given by [12]

$$f = f_1 \pm k f_r$$

are also related to air-gap eccentricity faults.

Besides the bearing fault characteristic frequency, vibration frequency components due to mechanical faults are also located at the first three harmonics of rotor speed, f_r, $2f_r$, and $3f_r$.

4. METHODS

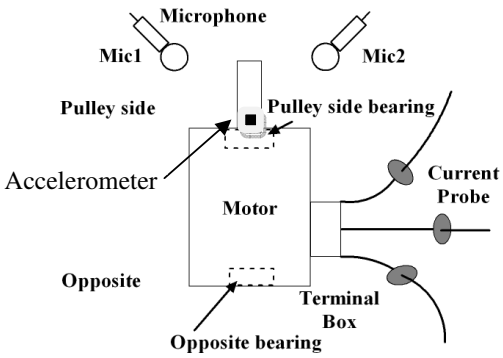

Fig. 1 Experiment setup diagram

Materials

This paper studies the current, vibration and sound signal collected from a 1.5 hp 3-phase induction motor with two faults: 1) air-gap eccentricity; 2) damaged outer race of bearings. The experiment setup is shown in Figure 1. The motor used here is rated at 230V line voltage and 4.8A line current. It is connected to an adjustable speed drive to control the speed. The current, vibration and sound signals are collected by a current probe, an accelerometer and 2 microphones respectively.

The effects of air-gap eccentricity are studied by replacing one of the bearings in the motor housing by a smaller outside diameter bearing covered with off-centered bushing (Figure 2). This causes a slope of the rotor center line as shown in Figure 3. The offset causes an uneven air-gap length between the rotor and the stator core thus resulting in eccentricity of the air-gap fault. The side view shows the air gap changing linearly between the rotor and stator core along the shaft axis. In Figure 3, L1 is the minimum air gap which is approximately 0.4 mm, and L2 is the maximum air gap which is approximately 0.8 mm.

Bearing faults are studied by replacing the pulley side bearing of the motor with an open bearing. The open bearing allows access to the race way of a bearing. This bearing is scratched using diamond mounted tool on the surface of outer race way.

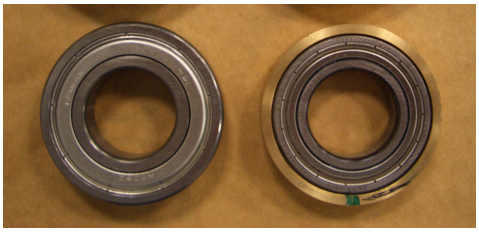

Fig. 2 Original opposite bearing and its replacement

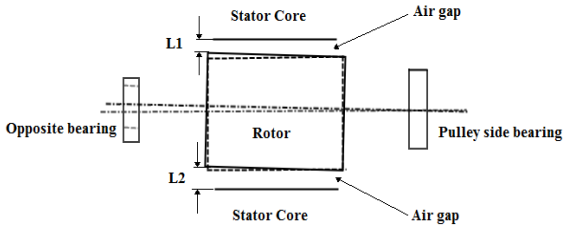

Fig.3 Uneven static air-gap eccentricity

Experimental Design

Table 1 Data sets summary

Sensor type	Sampling rate (Hz)	time duration per trial (second)	Total No. of trials for each condition
accelerometer	130	4	240
Current probe	8000	2	240
Microphone 1	4096	2	240
Microphone 2	4096	2	240

Experiments are conducted under four different conditions: only bearing fault condition, only air-gap eccentricity condition, both faults simultaneously and a normal control condition. For each condition, the motor is set up at least twice independently switched from one condition to another to collect the data. The running speed of the motor is 1200 rpm. The characteristics of the sensors and the experimental conditions are summarized in Table 1. The sound data are collected in 44.1 kHz sampling rate and downsampled to 4096 Hz. The electric current data is passed through a low pass filter with the cut-off frequency of 1500Hz. Current and microphone data are collected for 2 second durations whereas

the accelerometer data is gathered for 4 second durations. For each sensor, 240 sets of data are obtained.

Analysis

The Intrinsic Mode Functions (IMF) are extracted using the procedure outlined in Section 2. Since the sampling rate of the accelerometer is lower, there are fewer features from the vibration sensors. Only two IMFs are used in vibration data, seven IMFs are used in sound, and eight IMFs are used in current data analysis. The features selected for different sensor are listed in Table2. The features are then used as input to various classifiers discussed in the next section.

Table 2 Features list

Vibration data	Current data	Sound data
1f_r in IMF2	PSH in IMF1	PSH in IMF1
2f_r in IMF1	f_1+f_o in IMF2	f1+14fr in IMF1
3f_r in IMF1	f_1+6f_r in IMF3	f1+10fr in IMF2
Average value of IMF1 envelope	f_1+6f_r in IMF4	f1+13fr in IMF2
Total: 4 features	f_1+3f_r in IMF4	f1+12fr in IMF2
	f_1 in IMF5	f1+2fr in IMF3
	f_1+3f_r in IMF5	f1+3fr in IMF3
	f_1-f_o in IMF8	f1+4fr in IMF3
	Average value of IMF2 envelope	f1+5fr in IMF3
	Total: 9 features	f1+6fr in IMF3
		f1+7fr in IMF3
		f1+fo in IMF4
		f1 in IMF5
		fo in IMF5
		fr in IMF6
		f1-fo in IMF7
		average value of IMF4 envelope
		Total: 17 features

5. DATA ANALYSIS AND RESULTS

The Principal Slot Harmonic (PSH) can be calculated from equation 11. Since the rotor has 46 bars, the PSH frequency is approximately 979.8 Hz. The bearing is SKF bearing of series 6206. There are 9 balls in the bearing. The ball diameter is 10.8mm and the pitch diameter is 45.6mm. The outer race fault characteristic frequency is 68.8 Hz. These features are thrown into various classifiers, the results are shown below.

Figure 4 shows the IMFs of a typical vibration signal for 2 faults condition. The current and sound signals are decomposed similarly.

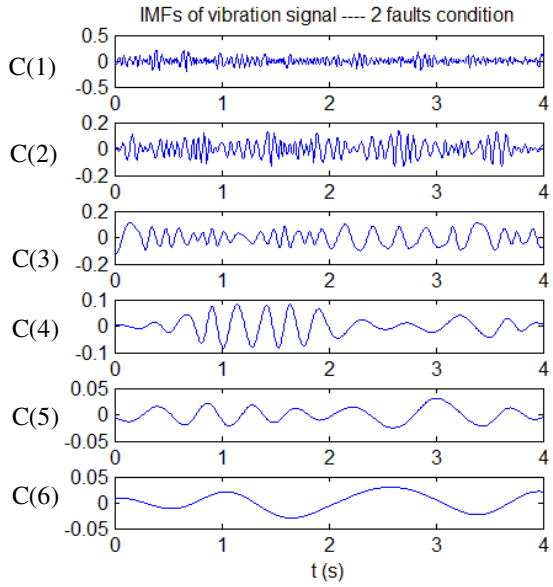

Fig.4 IMFs of vibration signal: 2 faults condition

Figure 5 compares the spectrum of original current signal and the IMF8. It is obvious the current spectrum does not show the peak of 9 Hz which is $|f_1-f_o|$, while the IMF8 spectrum shows clearly at the right frequency bin, which demonstrates that intrinsic mode 8 here is dominated by the bearing outer race fault. The 9 Hz frequency peak has the largest magnitude in the spectrum of IMF8.

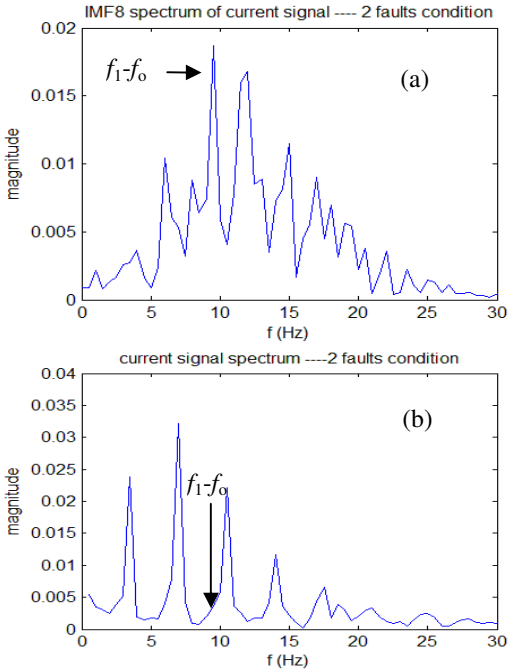

Fig. 5 (a) Spectrum of IMF8 (b) Spectrum of original current signal

The sound signal contains information that is contained in the current and vibration signals. Figure 6(a)

shows the zoomed spectrum of IMF4. The bearing fault frequency $f_1 + f_o$ (129 Hz) is clearly shown in the spectrum of IMF4 which is also shown in current spectrum. Figure 6(b) shows the zoomed spectrum of IMF5. The bearing fault characteristic frequency f_o (69 Hz) is easy to find. This frequency corresponds to the fault feature frequency in vibration spectrum. Compared to Figure 6(c), spectrum of original microphone 1 signal, the spectrum of IMF4 and IMF5 separates two feature frequencies in two modes and the peak is clearer than the ones in original signal spectrum.

The features described in Table 2 are used as input to simple classifiers. The three classifiers used are Naïve Bayesian (NB) classifier, k-Nearest Neighbor (k-NN) classifier and feed-forward back propagation Artificial Neural Network (ANN). 120 trials of each class are randomly selected as training data, and the remaining 120 trials are used as testing data. In order to demonstrate the effectiveness of the features described in Table 2, FFT features are also extracted and used as input to these classifiers. The comparison is carried out in all the classification tests.

Table 3 lists the results using only one of these sensors in the experiment. Current sensor itself can achieve 78.8% correct classification rate. Vibration sensor can only achieve 59.2% correct classification rate. This could be caused by the low sampling rate of vibration sensor and fewer features. Two microphones give similar classification rate results. Microphone 1 is slightly better because it is farther away from the noisy adjustable speed drive beside the terminal box whereas the microphone 2 was placed closer to the adjustable speed drive. Because of the low classification accuracy, multiple features are necessary.

Table 3. Correct classification rate of the testing data

Classifier \ Sensor		Accelero meter	Current probe	Micro-phone 1	Micro-phone 2
NB (%)	HHT	53.9	72.7	64.6	57.9
	FFT	30.8	61.0	60.8	56.5
k-NN (%)	HHT	52.3	70.0	**72.1**	70.0
	FFT	38.8	64.4	**74.6**	**74.2**
ANN (%)	HHT	**59.2**	**78.8**	71.9	**71.3**
	FFT	**49.4**	**65.6**	71.9	65.8

Table 4 shows the results tested using features from two sensors. The features from different sensors are simply accumulated in a feature vector. The performance is greatly improved by using two sensor features. The vibration sensor and current sensor can achieve 88.9% correct classification rate which is higher than the performance of vibration with sound sensor features. This is reasonable because single current sensor has higher performance than single sound sensor in Table 3. Table 4 shows the results of best combination of two sensor features which the combination of two microphone sensors. The performance can be increased to 99.2% correct classification rate using k-NN classifier. The other 2 classifiers also have high classification rates.

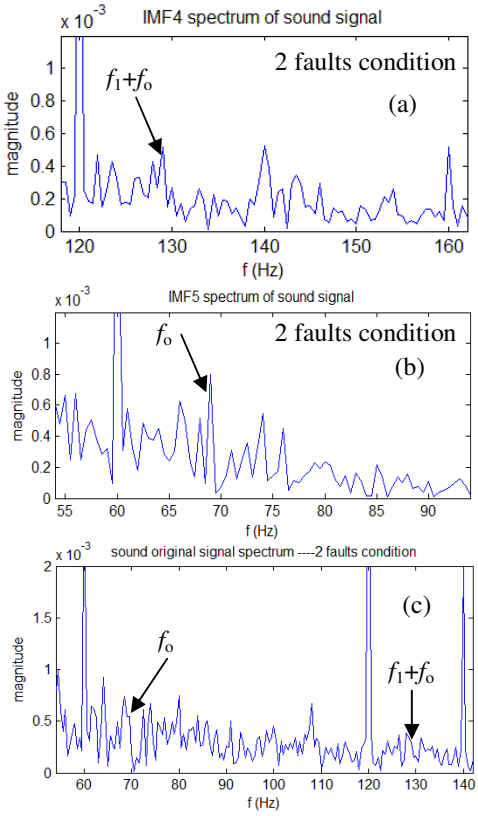

Fig. 6 (a) Spectrum of IMF4 (b) Spectrum of IMF5 (c) Spectrum of original microphone 1

Table 4 Classification results using two sensors

Sensors* \ Correct Classification Rate (%)	NB		k-NN		ANN	
	HHT	FFT	HHT	FFT	HHT	FFT
ACC + CP	76.7	**70.0**	66.7	58.5	**88.9**	65.6
ACC +Mic1	66.9	62.1	69.0	**77.9**	**71.0**	71.7
ACC+ Mic2	**84.0**	72.3	73.5	**71.3**	75.6	**71.3**
CP + Mic1	90.4	76.3	77.9	77.3	**96.7**	**93.3**
CP + Mic2	79.0	70.2	91.5	75.6	**95.7**	**90.4**
Mic1 + Mic2	98.5	71.7	**99.2**	**93.3**	96.0	93.1

*ACC: accelerometer; CP: Current Probe; Mic: Microphone

Table 5 lists the classification results using all combinations of three sensors' features and all sensors' features. The performance of all combinations are higher than most of two sensor results. Two microphones with vibration or current sensor can achieve above 90% correct classification using all

the classifiers. With all sensors used, the performance can achieve 99.8% correct classification rate using ANN classifier. From all the testing above, very few of FFT features get higher classification rate.

Table 5. Classification results using three or more sensors

Sensors	Correct Classification Rate (%)					
	NB		k-NN		ANN	
	HHT	FFT	HHT	FFT	HHT	FFT
ACC + CP + Mic1	94.4	76.5	67.3	64.6	**97.5**	**93.5**
ACC+CP+ Mic2	88.3	70.2	80.7	87.1	**99.4**	**93.5**
ACC+Mic1 +Mic2	**99.2**	**74.2**	93.3	70.6	96.7	70.6
CP+Mic1+ Mic2	97.3	79.0	94.0	81.7	**99.6**	**94.4**
ACC+CP+ Mic1+Mic2	98.3	72.7	81.3	88.5	**99.8**	**96.7**

6. CONCLUSIONS

This paper described the empirical mode decomposition based method for the detection of multiple faults in induction motors. Two faults are studied 1) Air-gap eccentricity 2) Defective outer race in bearings. The experiments are conducted under no-fault, single fault and multiple faults condition. The results demonstrate the effectiveness of using intrinsic mode functions in Hilbert-Huang transform to construct features for classification. However, no single sensor was able to achieve a high enough classification accuracy. Multiple sensors were required to enable reliable classification.

Air-gap eccentricity and defective bearing outer-race are two of several faults that can occur in motors. The other faults include rotor bar failures, winding problems, and bearing problems that are caused by other defects such as pitting or inner race damage. Future work will expand upon the methods of this paper to uncover these faults using multi-sensor fusion methods.

ACKNOWLEDGMENTS

The authors would like to thank Dr. Wallace Brithinee, Dr. Donald Brithinee and Bill Butek of Brithinee Electric Inc. located in Colton, California, for their support with equipment and expertise. We would also like to thank graduate student Rafael Garcilazo to help for the experiments.

REFERENSES

[1] J. R. Cameron, W. T. Thomson, and A. B. Dow, "Vibration and current monitoring for detecting airgap eccentricity in large induction motors," *Electric Power Applications, IEE Proceedings B,* vol. 133, pp. 155-163, 1986.

[2] D. G. Dorrell, W. T. Thomson, and S. Roach, "Analysis of airgap flux, current, and vibration signals as a function of the combination of static and dynamic airgap eccentricity in 3-phase induction motors," *Industry Applications, IEEE Transactions on,* vol. 33, pp. 24-34, 1997.

[3] Z. Wei, T. G. Habetler, and R. G. Harley, "Bearing Condition Monitoring Methods for Electric Machines: A General Review," in *Diagnostics for Electric Machines, Power Electronics and Drives, 2007. SDEMPED 2007. IEEE International Symposium on*, 2007, p. 3.

[4] B. Li, M. Y. Chow, Y. Tipsuwan, and J. C. Hung, "Neural-network-based motor rolling bearing fault diagnosis," *Industrial Electronics, IEEE Transactions on,* vol. 47, pp. 1060-1069, 2000.

[5] R. R. Schoen, T. G. Habetler, F. Kamran, and R. G. A. B. R. G. Bartfield, "Motor bearing damage detection using stator current monitoring," *Industry Applications, IEEE Transactions on,* vol. 31, p. 1274, 1995.

[6] Z. K. Peng, P. W. Tse, and F. L. Chu, "A comparison study of improved Hilbert-Huang transform and wavelet transform: Application to fault diagnosis for rolling bearing," *Mechanical Systems and Signal Processing,* vol. 19, pp. 974-988, 2005.

[7] V. K. Rai and A. R. Mohanty, "Bearing fault diagnosis using FFT of intrinsic mode functions in Hilbert-Huang transform," *Mechanical Systems and Signal Processing,* vol. 21, pp. 2607-2615, 2007.

[8] B. Liu, S. Riemenschneider, and Y. Xu, "Gearbox fault diagnosis using empirical mode decomposition and Hilbert spectrum," *Mechanical Systems and Signal Processing,* vol. 20, pp. 718-734, 2006.

[9] L. Hui and Z. Haiqi, "Bearing Fault Detection Using Envelope Spectrum Based on EMD and TKEO," in *Fuzzy Systems and Knowledge Discovery, 2008. FSKD '08. Fifth International Conference on*, 2008, pp. 142-146.

[10] N. E. Huang, Z. Shen, S. R. Long, M. L. C. Wu, H. H. Shih, Q. N. Zheng, N. C. Yen, C. C. Tung, and H. H. Liu, "The empirical mode decomposition and the Hilbert spectrum for nonlinear and non-stationary time series analysis," *Proceedings of the Royal Society of London Series a-Mathematical Physical and Engineering Sciences,* vol. 454, pp. 903-995, Mar 1998.

[11] N. Huang, M. Wu, S. Long, S. Shen, W. Qu, P. Gloersen, and K. Fan, "A confidence limit for the empirical mode decomposition and Hilbert spectral analysis," *Royal Society of London Proceedings Series A,* vol. 459, pp. 2317-2345, 2003.

[12] S. Nandi and H. A. Toliyat, "Condition monitoring and fault diagnosis of electrical machines-a review," in

Industry Applications Conference, 1999. Thirty-Fourth IAS Annual Meeting. Conference Record of the 1999 IEEE, 1999, p. 197.